Journal of Optoelectronic and Biomedical Materials Vol. 17, No. 3, July -September 2025, p. 141 - 149

# Study of structural/microstructural and optical characteristics of tin oxide ($SnO_2$) thin film grown at different substrate temperatures of 325 °C, 375 °C, 425 °C by spray pyrolysis method

A. Verma *, K. Shriram, B. Das
*Department of Physics, University of Lucknow, Lucknow (U.P.), 226007, India*

Tin oxide is a promising candidate for high-impact applications in optoelectronic devices. The main purpose of this paper is to discuss the systematic study of the preparation of tin oxide thin film (spray pyrolysis technique) with variations at glass substrate temperatures of *325* ℃*, 375* ℃*, 425* ℃. X-ray diffraction pattern reveals that $SnO_2$ has a polycrystalline tetragonal-shaped structure with space group $P4_2/mnm$. Crystallite size, lattice parameter, and lattice strain were increased with increasing substrate temperature. Scanning Electron Microscopy/Atomic Force Microscopy images show that cuboid-shaped particles with few pores are distributed over the surface. AFM also demonstrated the root means square roughness was varying from 0.285nm - 0.290nm. RAMAN spectroscopy identifies primarily $A_{1g}$, $B_{2g}$,, doubly degenerate $E_g$ vibrational modes in thin films.

(Received March 27, 2025; Accepted July 8, 2025)

*Keywords:* $SnO_2$, Thin film, Spray pyrolysis method, Structural and optical properties

## 1. Introduction

During the last few years, tin oxide nanomaterials have had great demand in the field of chemical, electronic, and pharmaceutical industries because they have venerable properties like electrical, optical, magnetic, and thermal properties. It is an n-type semiconductor with a wide bandgap (3.6 eV) at 300k. Further, low resistivity, high chemical, mechanical, and thermal stability are essential properties [1]. It is applicable in perovskite solar cells, gas sensors, lithium-ion batteries, optoelectronic devices, and also liquid crystal displays [2-6]. Another application of tin oxide is in the automotive sector as an anticorrosive surface treatment of a carbonaceous bipolar plate in proton exchange membrane fuel cells [7]. There are various types of synthesis techniques for tin oxide thin film such as spin coating [8], thermal evaporation [9], pyrosol process [10], hydrothermal method [11], chemical precipitation method [12], sol-gel method [13], etc.

Several scholars have reported innovative research on tin oxide nanomaterial, which we discussed here briefly. Zhang G. et al. have prepared thin film of tin oxide nanomaterial by sol-gel process. He says crystallization of said material started at 250°$C$ and nanocrystalline tin oxide powder was formed at nearly 600°$C$ only after the hydroxyl group has been fully removed [7, 14]. Satori Baco, et al. worked on different annealing temperatures (373-673) °$C$ of tin oxide, which was synthesized by radio frequency sputtering technique. It was found that samples exhibited higher transparency of more than 70% in visible light and the bandgap was decreased with increasing annealing temperature [15]. M. H. Haja Sheriff, et al. have reported their study on the influence of sintering temperature (300-500) °$C$ on structural and optical properties of tin oxide thin film. In this way, various methods like XRD, SEM, UV-Vis spectroscopy, and RAMAN spectroscopy have been used. XRD result shows that all peaks are clear and sharp at a substrate temperature of 400°$C$, and optical absorption spectra revealed that the maximum absorption was absorbed at 400°$C$. From the SEM images, we can say that the surface morphology was changed with the increasing temperature of the substrate [16]. H. S. Wasley et al prepared tin oxide thin film by thermal evaporation technique and explored the structural, morphological, and optical properties of their samples. XRD pattern indicates the thin film was an amorphous nature and

* Corresponding author: archanaverma8631@gmail.com
https://doi.org/10.15251/JOBM.2025.173.141

RAMAN spectroscopy confirms the formation of tin oxide nanomaterials. AFM images show the particles are well connected and distributed through all surfaces and a direct band gap of tin oxide was found 3.49 eV from UV-Vis spectroscopy [17]. Selma M. H. Al-Jawad et al observed based on their research, that tin oxide film has an orthogonal structure at a low-temperature substrate and a tetragonal structure at a high-temperature substrate [18]. On the other hand, much literature regarding transition metal doped tin oxide [19, 20, 21] and we conclude that if we doped transition metal in tin oxide, the properties of tin oxide were improved.

Therefore, the current research has been chosen by the above encouraging experimental data to discuss the systematic study on the preparation (spray pyrolysis method) of tin oxide ($SnO_2$) thin film with variation in glass substrate temperature at *325* ℃*, 375* ℃*, 425* ℃ and annealed at 450 ℃ for 1 hour**.** Samples have been characterized by XRD (X-ray diffraction), SEM (Scanning electron microscopy), AFM (Atomic force microscopy), and RAMAN spectroscopy.

## 2. Experimental details

The thin film of pure tin oxide was prepared by the spray pyrolysis method. In this process, substrate temperature plays an important role, so we decided that the substance temperature was $325°C$ to get clear film. When the substrate temperature is below $300°C$, the spray falling on the substrate will undergo incomplete thermal decomposition giving rise to a foggy film whose transparency will be very poor. If the substrate temperature is high ($500°C$) the spray gets vaporized before reaching the substrate and the film becomes powdery.

For the 0.1 M solution, we took a proper amount of high-purity raw material tin chloride dehydrates ($SnCl_2.2H_2O$) (Sigma Aldrich, purity > 99.99%) diluted in distilled water and added a few drops of concentrated Hydrochloric acid (Merck, Min 35 % GR). Because the intermediate polymer molecules broke down, we needed a transparent solution, thus we utilized HCl as a solvent [22]. The solution was stirred by a magnetic stirrer for 1 hour to obtain a homogeneous solution. The glass substrates were sprayed with this solution. As a result, the 10 mm × 10 mm ×1.1 mm clean glass slides were utilized as substrates. The substrate was heated at 325 $°C$, 375 $°C$, and 425 $°C$, and the temperature was controlled by an electronic temperature controller, which was connected to the heater. During deposition, the flow rate of solution was at 0.2 ml/min by nebulizer (particle size 0.5-10 micrometers). Nozzle and substrate were maintained at a distance of 30 Cm and spray time was about 3 min for each film. All samples were annealed at $450°C$ for 1 hour and after that, it cooled down to room temperature. Table 1 illustrates some process parameters for the preparation of tin oxide thin film grown at different substrate temperatures *(325* ℃*, 375* ℃*, 425* ℃) by spray pyrolysis method.

To determine how the substrate temperature *(325-425)* $°C$ affects the structural/microstructural and optical properties of tin oxide's thin film. The method used for the preparation of tin oxide thin films was spray pyrolysis and finally, samples were characterized by X-ray diffractometer (XRD), Scanning Electron Microscope (SEM), AFM (Atomic Force Microscopy), and RAMAN spectroscopy. The gross structure and chemical phase determination of nanomaterials were carried out by Powder X-ray diffractogram (Rigaku ultima IV) operating with Cu-Kα radiation (λ = 0.15406 nm) at 45 kV and 40 mA at a scan angle ($2\theta$) of 20–80 $°C$ at a scanning rate of 1.5°/minute. RAMAN spectroscopy (Jobin Yvon Horibra LABRAM-HR 800 visible) was performed in the range of 200-1200 $cm^{-1}$ using a He-Ne laser source to inspect the chemical vibrational bonding of each element in samples. To identify the surface morphology of thin film, a Scanning electron microscope (Gemini SEM 300) was used in this investigation. Surface topography and root mean square (RMS) roughness have been examined by atomic force microscopy (Digital instrument nanoscope E AFM from DI, USA). The maximum scan area for getting the image was 10 × 10 $micrometer^2$.

*Table 1. Illustrates some process parameters for the preparation of tin oxide thin film grown at different substrate temperatures (325 °C, 375 °C, 425 °C) by spray pyrolysis method.*

| | |
|---|---|
| **Substrate temperature** | 325 °C, 375 °C, 425 °C |
| **Distance between nozzle to substrate** | 30 Cm |
| **Time of deposition for each film** | 3 min |
| **Solution (tin chloride dehydrates) concentration** | 0.1 M |
| **Temperature of annealing** | 450 °C |
| **Time of annealing** | 1 hour |
| **Used solvent** | water |

## 3. Results and discussion

### 3.1. Structural morphology

#### *3.1.1. XRD (X-ray diffraction analysis)*

Fig. 1(a) indicates that XRD patterns of tin oxide thin film at different substrate temperatures 325 $°C$, 375 $°C$, and 425 $°C$, which prove that tin oxide has a tetragonal rutile structure with space group $P4_2/mnm$ and no peaks concerning to impurity nor any secondary phase of $SnO_2$ has detected. It was confirmed by JCPDS NO- 00-021-1250. The distinctive peaks were positioned at 2θ = 26.5, 33.6, 37.8, 51.6 having (h k l) values of (110), (101), (200), (211). These peaks fit with previous work [22]. Peak (110) was found to be the most intense peak compared with three other peaks. This peak is attributed to the density of atoms in the (110) plane, which was highest in rutile type crystallite structure, and surface energy was found to be the lowest order in the (110) plane [23]. XRD pattern of thin film prepared at a substrate temperature of 325 $°C$ shows a low-intensity peak means the thin film is non-crystalline. When substrate temperature was increased to 375 $°C$ and 425 $°C$ , XRD peaks became more intense and had good crystallinity. We observed that crystallinity increases with the increasing substrate temperature of the thin film. The average crystallite size has been deliberated using Debye Scherer's formula [24].

$$\text{Crystallite size (D)} = \frac{0.9\lambda}{\beta \cos\theta} \tag{1}$$

where β is the full width at half maximum (FWHM) that corresponds to the diffraction angle 2θ (θ is Bragg's angle) and λ is the wavelength of Cu Kα radiation (1.5406 A°) at a scanning rate of $1^0$/min. The calculated average crystallite size was found to be in the range of 3.12 nm - 17.0 nm, which is shown in Table 2. It was noticed that the average crystallite size was increasing with the rising temperature of the substrate due to improvement in the crystallinity of the thin film. The same result behalf of this [25]. Therefore, the intensity of the peak was also increasing and decreasing full width at half maxima (FWHF) as well as up to higher substrate temperature. Because they have enough energy available to them, the tin oxide particles can combine to produce larger particles [26]. This is dependent on the synthesis process, deposition conditions, atmosphere, etc. Williamson-Hall (W-H) plots additionally provide crystallite size value and lattice strain value using this formula [27].

$$\beta\cos\theta = \frac{k\lambda}{D} + 4\varepsilon\sin\theta \tag{2}$$

Because the Bragg diffraction peak width combines the width broadening caused by the materials with the instrumental integral width. Consequently, the following formula is used to determine the proper broadening of the sample's diffraction peak [28].

$$\beta = [\beta^2_{measure} - \beta^2_{instrumental}]^{1/2} \tag{3}$$

Diffraction data of standard material (such as silicon, etc.) was used to find out the instrumental integral width ($\beta_{instrumental}$), where β is full width at half maxima and ε is lattice

microstrain and D is crystallite size. If we linear fit to the data of the graph plot between βCosθ and 4Sinθ (known as Williamson-Hall plots), the inverse of the intercept gives crystallite size and the slope gives lattice strain value. The lattice strain values of $SnO_2$ thin film at different substrate temperatures 325 °*C*, 375 °*C*, and 425 °*C* were found to be $-7.51\times10^{-4}$, $-3.22\times10^{-3}$, $6.30\times10^{-3}$ respectively are given in Table 3 and see fig. 1(b). We observed that crystallite size calculated from Debye Scherer's formula was very near the W-H plot.

For the tetragonal structure, the lattice parameter has been calculated using this relation given below-

$$\frac{1}{d^2} = \frac{(h^2+k^2)}{a^2} + \frac{(l^2)}{c^2} \tag{4}$$

Here a, b, and c are lattice parameters and it is given in Table 3. We noticed that the lattice parameter was increasing with the raising substrate temperature of thin films. So that lattice should be expanded. The formula of cell volume of the tetragonal structure is $a^2\times c$, here a and c are lattice parameters, and it was listed in Table 3.

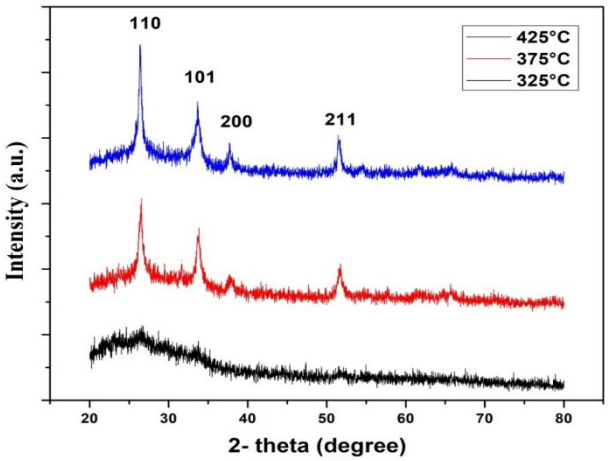


*Fig. 1 (a) X-ray diffraction (XRD) pattern of tin oxide thin film gown at different substrate temperatures of 325 °C, 375 °C, 425 °C.*

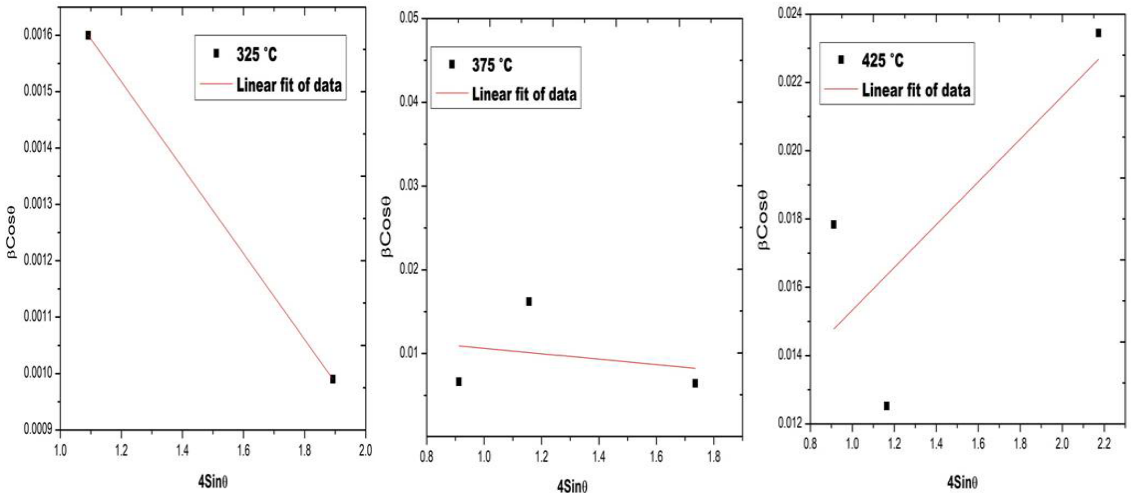


*Fig. 1. (b) W-H plot of tin oxide thin film gown at different substrate temperatures of 325 °C, 375 °C, 425 °C.*

*Table 2. Average crystallite size (nm) of tin oxide thin film at different substrate temperatures of 325 °C, 375 °C, 425 °C.*

| Substrate temp. of $SnO_2$ thin film | Average crystallite value (nm) | | |
|---|---|---|---|
| | Scherer's | W-H plot | SEM |
| ***325 °C*** | 3.12 | 5.20 | - |
| ***375 °C*** | 8.25 | 10.66 | 45.2 |
| ***425 °C*** | 15.30 | 17.0 | - |

*Table 3. The lattice parameters (a, b, c), cell volume, lattice strain, and dislocation density of tin oxide thin film grown at different substrate temperatures of 325 °C, 375 °C, 425 °C.*

| Substrate temp. of $SnO_2$ thin film | Lattice parameter a=b ($\AA$) | c ($\AA$) | Cell Volume ($\AA$)$^3$ | Dislocation density (nm$^{-2}$) | Lattice strain ($\varepsilon$) |
|---|---|---|---|---|---|
| **325 °C** | 4.718 | 3.170 | 70.562 | $1.02\times10^{-1}$ | $7.51\times10^{-4}$ |
| **375 °C** | 4.727 | 3.178 | 71.010 | $1.46\times10^{-2}$ | $3.22\times10^{-3}$ |
| **425 °C** | 4.735 | 3.198 | 71.699 | $4.27\times10^{-3}$ | $6.30\times10^{-3}$ |

### 3.2. Surface morphology and topography analysis

#### *3.2.1. Scanning electron microscopy (SEM)*

To study the surface morphology (shape and size) of particles, SEM has been done in the present investigation. The optical and electronic properties are enhanced by the surface morphology of transparent conducting oxide for the applications of optoelectronic devices. Therefore, surface morphology of thin film becomes necessary [16]. Fig. 2 demonstrates the SEM images of the thin film at the substrate temperature of *375 °C* and the image was analyzed by IMAGE-J software. The average particle size was found that 45.2 nm with cuboid-shaped and particles were dispersed across all surfaces. Table 2 demonstrates the comparison between grain size values estimated from XRD and SEM.

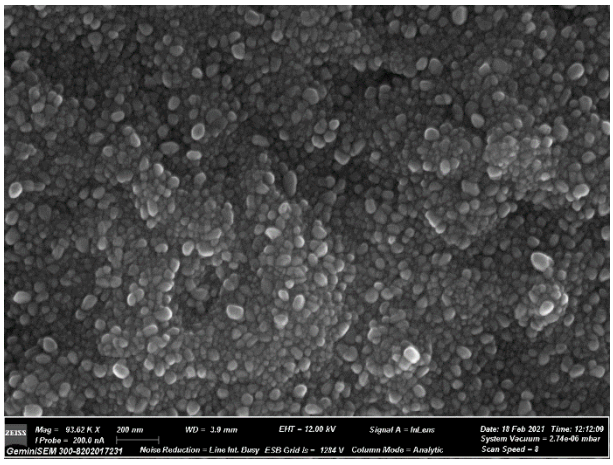


*Fig. 2. Scanning electron microscopy (SEM) of tin oxide thin film gown at substrate temperatures of 375 °C.*

### *3.2.2. Atomic force morphology (AFM)*

The surface topography of tin oxide thin film at different substrate temperatures (325°$C$, 375°$C$, 425°$C$) has been explored through Atomic Force Morphology (AFM) by using WSxM software. These images (see Fig. 3) show that particle size has been increasing from 33 nm to 86 nm with increasing substrate temperature of samples. The particle size calculated from AFM\SEM is higher than XRD measurement because XRD data shows average mean size crystallites and AFM\SEM gave agglomeration of crystallites. The calculated root mean square roughness (RMS), average roughness, and particle size are shown in Table 4.

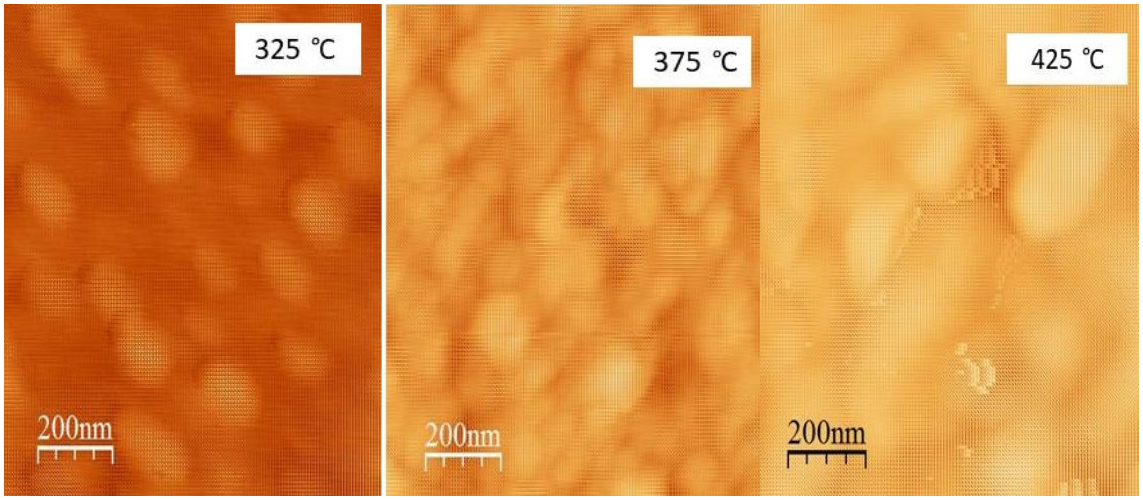


*Fig. 3. Atomic force morphology (AFM) of tin oxide thin film gown at different substrate temperatures of 325 °C, 375 °C, 425 °C.*

*Table 4. The calculated root means square roughness (RMS) and average roughness of tin oxide thin film at different substrate temperatures of 325 °C, 375 °C, and 425 °C.*

| **Substrate temp. Of $SnO_2$ thin film** | **RMS Roughness (nm)** | **Average Roughness (nm)** | **Particle Size (nm)** |
|---|---|---|---|
| **325 °$C$** | 0.285 | 0.245 | 33 |
| **375 °$C$** | 0.288 | 0.247 | 40 |
| **425 °$C$** | 0.290 | 0.249 | 86 |

## 3.3. Optical properties

### *3.3.1. RAMAN spectroscopy*

The crystal structure and vibrational mode (VM) of a thin film of tin oxide have been observed using RAMAN spectroscopy in the frequency range (100-1300) $Cm^{-1}$ at various substrate temperatures, including 325°C, 375°C, and 425°C. Two tin and four oxygen atoms with a point group of $D_{4h}^{14}$ and a space group of $P4_2/mnm$ made up the tetragonal-shaped crystal structure of tin oxide. The $SnO_2$ system has a total of eighteen vibrational modes, according to group theory. The normal modes are 3n (since the primitive cell of $SnO_2$ has 6 atoms). From Fig. 4, we observe that there was a weak peak at 113.2 $cm^{-1}$, which corresponded to the $B_{1g}$ mode [29]. Additionally, a weak peak of the $E_g$ doubly degenerate mode, caused by the oxide ion vibration mode, is visible at 476 $cm^{-1}$ [30]. The expansion or contraction dispersion of the Sn-O bonds is responsible for the tiny band at 776.6 $cm^{-1}$ in the $B_{2g}$ Raman active mode [30]. The presence of a $E_u$ signal from the IR active mode at 556 $cm^{-1}$ may be related to oxygen ion vacancies [30]. Furthermore, a large peak at 1093 $cm^{-1}$ may be associated with the $Sn\text{-}O_2$ bands' stretching vibrational modes [30].

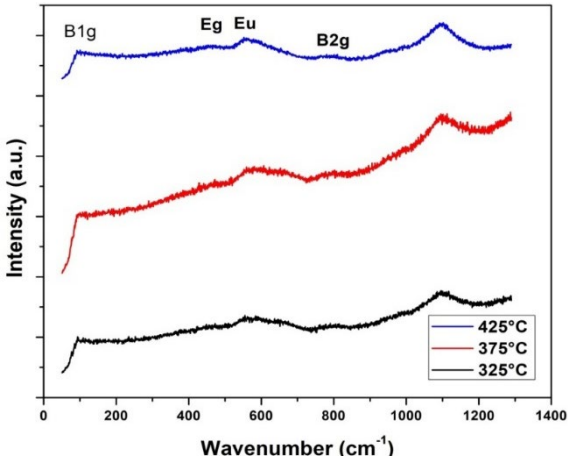


*Fig. 4. Raman spectroscopy of tin oxide thin film gown at different substrate temperatures of 325 °C, 375 °C, 425 °.*

*Table 5. Raman active mode of tin oxide thin film gown at different substrate temperatures of 325 °C, 375 °C, 425 °C.*

| Vibration mode in $SnO_2$ thin film | *325 °C* | *375 °C* | *425 °C* |
|---|---|---|---|
| $B_{1g}$ | 113.2 | 113.5 | 113.9 |
| $E_g$ | 476.6 | 476.8 | 476.9 |
| $B_{2g}$ | 776.6 | 776.9 | 777.0 |

## 4. Conclusion

In summary, this paper discusses the elaboration of tin oxide thin film on a glass substrate by using the spray pyrolysis technique and investigates the influence of substrate temperature (325°C, 375°C, 425°C) on structural/microstructural and optical properties of tin oxide thin film with the help of different ways. From the obtained results, the XRD pattern and RAMAN spectroscopy reveal that $SnO_2$ has a polycrystalline tetragonal-shaped structure with space group $P4_2/mnm$. Because the thin film's crystallinity has improved, we find that the average crystallite size has grown when the substrate's temperature has increased. According to the SEM image, the nanoparticles at 375 °C had a cuboid form and an average size of 45 nm. Additionally, the cuboid-shaped particles with few pores are shown by AFM measurement. Three vibrational modes ($A_{1g}$, $B_{2g}$, and doubly degenerate $E_g$) are primarily identified in all samples using RAMAN spectroscopy.

### Acknowledgments

We acknowledge analysis support from Dr. Vasant G. Sathe, Centre-Director of UGC-DAE Consortium for Scientific Research (Indore, India.), and We are also thankful to Late Dr. Piyush Jaiswal (Physics department), Prof. M. K. Dutta (Director Centre of Advanced Studies), Dr. A.P.J.A.K.T.U (Lucknow, India) for measurements.

## Availability of data and materials

The raw data can be obtained on request from the corresponding author.

## References

[1] Q. Ye, X. Zhang, R. Yao, D. Luo, X. Liu, Crystals 11(12), 1479 (2021); https://doi.org/10.3390/cryst11121479

[2] G. Lucarelli, T. M. Brown, Frontiers in Materials 6, 310 (2019); https://doi.org/10.3389/fmats.2019.00310

[3] Y. Masuda, Sensor and actuators B: Chemical 364, 131876 (2022); https://doi.org/10.1016/j.snb.2022.131876

[4] X. W. Lou, C. M. Li, L. A. Archer, Advanced Materials 21, 2536 (2009); https://doi.org/10.1002/adma.200803439

[5] H. Heffner, M. Soldera, A. F. Lasagni, Scientific Reports 13(1), 9798 (2023); https://doi.org/10.1038/s41598-023-37042-y

[6] M. Souada, C. Louage, Jean.Y. Doisy, L. Meunier, A.Benderrag, B. Ouddane, S. Bellayer, N. Nuns, M. Traisnel, U. Maschke, Ultrasonics Sonochemistry 40, 929 (2018); https://doi.org/10.1016/j.ultsonch.2017.08.043

[7] N. Abdullah, N. M. Ismail, D. M. Nuruzzaman, Materials Science and Engineering 319, 012022 (2018); https://doi.org/10.1088/1757-899X/319/1/012022

[8] N. Huster, D. Zanders, S. Karle, D. Rogalla, A. Devi, Dalton Transactions 49(31), 10755 (2020); https://doi.org/10.1039/D0DT01463J

[9] H. W. Kim, S. H. Shim, C. Lee, Ceramics International 32(8), 943 (2006); https://doi.org/10.1016/j.ceramint.2005.06.015

[10] A. Smith, J. M. Laurent, D. S. Smith, J. P. Bonnet, R. R. Clemente, Thin Solid Films 266(1), 20 (1995); https://doi.org/10.1016/0040-6090(95)06648-9

[11] M. A. M. Akhir, S. A. Rezan, K. Mohamed, M. M. Arafat, A. S. M. A. Haseeb, H. L. Lee, Materials Today: Proceedings 17, 810 (2019); https://doi.org/10.1016/j.matpr.2019.06.367

[12] N. Yongvanich, S. Maensiri, Integrated Ferroelectricity 156, 53 (2014); https://doi.org/10.1080/10584587.2014.906278

[13] Y. Tao, P. P. Pescarmona, Catalysts. 8(5), 212 (2018); https://doi.org/10.3390/catal8050212

[14] G. Zhang, M. Liu, Journal of Material Science 34, 3213 (1999); https://doi.org/10.1023/A:1004685907751

[15] S. Baco, A. Chik, F. M. Yassin, Journal of Science and Technology 4(1), (2012).

[16] M. H. H. Sheriff, S. Murugan, A. Victor Babu, International Journal Advanced Research Engineering and Technology 12(3), 61 (2021).

[17] H. S. Wasly, M. S. A. E. Sadek, S. Elnobi, A. A. Abuelwafa, The European Physical Journal Plus 137(1), 1 (2022); https://doi.org/10.1140/epjp/s13360-022-02349-8

[18] S. M. H. Al-Jawad, F. H. Oleiwe, J. H. Khulaef, Engineering & Technical Journal 33(3), (2015); https://doi.org/10.30684/etj.33.3B.12

[19] N. H. Hong, J. Sakai, W. Prellier, A. Hassiniet, Journal of Physics: Condensed Matter 17(10), 1697 (2005); https://doi.org/10.1088/0953-8984/17/10/023

[20] N. Ahmad, S. Khan, M. M. N. Ansari, Ceramics International 44(13), 15972 (2018); https://doi.org/10.1016/j.ceramint.2018.06.024

[21] M. Duhan, N. Kumar, A. Gupta, A. Singh, H. Kaur, Vacuum 181, 109635 (2020); https://doi.org/10.1016/j.vacuum.2020.109635

[22] S. Gupta, V. Ganesan, I. Sulania, B. Das, Surface Science 664, 137 (2017); https://doi.org/10.1016/j.susc.2017.06.006

[23] A. Abdelkrim, S. Rahman, K. Nabila, A. Hafida, O. Abdelouahab, Journal of Materials Science: Materials in Electronics, 28(6), 4772 (2017); https://doi.org/10.1007/s10854-016-6122-9

[24] A. Verma, B. Das. Pramana-Jornal of Physics, 98(3), 88 (2024); https://doi.org/10.1007/s12043-024-02778-3

[25] M. V. Arularasu, M. Anbarasu, S. Poovaragan, R. Sundaram, K. Kanimozhi, C. Maria Magdalane, K. Kaviyarasu, F. T. Thema, D. Letsholathebe, G. T. Mola, M. Maaza, Journal of Nanoscience and Nanotechnology 18(5), 3511 (2018); https://doi.org/10.1166/jnn.2018.14658

[26] S. Naz, I. Javid, S. Konwar, K. Surana, P. K. Singh, M. Sahni, SN Applied Science 2, 1 (2020); https://doi.org/10.1007/s42452-020-2812-2

[27] R. R. Awasthi, B. Das, Optik 194, 162973 (2019); https://doi.org/10.1016/j.ijleo.2019.162973

[28] R. R. Awasthi, K. Asokan, B. Das, Applied Physics A 125(5), 338 (2019); https://doi.org/10.1007/s00339-019-2560-6

[29] D. Degler, Spectroscopic Insights in the Gas Detection Mechanism of Tin Dioxide Based Gas Sensors, Universität Tübingen, (2017).

[30] M. A. Y. Barakat, M. Shaban, A. M. El-Sayed, Material Research Express 5(6), 066407 (2018); https://doi.org/10.1088/2053-1591/aac80a